Vibronic Structure and Ion Core Interactions in Rydberg States of Diazomethane: An Experimental and Theoretical Investigation

Igor Fedorov, Lucas Koziol, Guosheng Li, Hanna Reisler,* and Anna I. Krylov*

Department of Chemistry, University of Southern California, Los Angeles, California 90089-0482

Received: August 24, 2007; In Final Form: October 10, 2007

Vibronic transitions to the $2^1A_2(3p_y \leftarrow \pi)$ Rydberg state of CH_2N_2, CD_2N_2, and $CHDN_2$ were recorded by 2 + 1 REMPI spectroscopy, and kinetic energy distributions (eKE) of photoelectrons from ionization of selected vibronic levels were determined by velocity map imaging. Normal-mode frequencies were obtained for the $2^1A_2(3p_y)$ Rydberg state and for the cation. Mixed levels of the $2^1A_2(3p_y)$ and $2^1B_1(3p_z)$ of the three isotopologs were identified by photoelectron imaging and analyzed. The equilibrium geometries and harmonic vibrational frequencies of the electronic states of neutral diazomethane were calculated by CCSD(T)/cc-pVTZ, and B3LYP/6-311G(2df,p). The latter method was also used to calculate isotope shifts for the ground-state neutral and cation. Geometry and frequencies of the ground state of the cation were calculated by CCSD(T)/cc-pVTZ, using the unrestricted (UHF) reference. The equilibrium structures, frequencies, and isotope shifts of the $2^1A_2(3p_y)$ and $2^1B_1(3p_z)$ Rydberg states were calculated by EOM-EE-CCSD/6-311(3+,+)G(2df). In all cases where comparisons with experimental results were available, the agreement between theory and experiment was very good allowing a full analysis of trends in structure and vibrational frequencies in going from the neutral species to the excited Rydberg states, $2^1A_2(3p_y)$ and $2^1B_1(3p_z)$, and the cation. Although the $2^1A_2(3p_y)$ and $2^1B_1(3p_z)$ states have planar C_{2v} symmetry like the ion, they exhibit differences in geometry due to the specific interactions of the electron in the $3p_y$ and $3p_z$ orbitals with the nuclei charge distributions of the ion core. Moreover, trends in normal-mode frequencies in the ground states of the neutral and ion and the $2^1A_2(3p_y)$ and $2^1B_1(3p_z)$ Rydberg states are consistent with removing an electron from the bonding π_{CN}-orbital, which also has an antibonding character with respect to NN. To explain the observed trends, the vibrational modes are divided into two groups that involve displacements mainly (i) along the CNN framework and (ii) in the CH_2 moiety. Trends in the first group are due mostly to the effect of the lower CN and NN bond orders, whereas those in the second group are due to the interaction between the positively charged hydrogens and the Rydberg electron density, and the hybridization of the carbon. Within each group, marked differences in behavior between the in-plane and out-of-plane modes are observed.

1. Introduction

Diazomethane (CH_2N_2) has been the subject of considerable interest, because its photolysis and pyrolysis provide efficient sources of singlet and triplet methylene,[1] and its spectroscopy is important for the formation of molecules in N_2-rich media such as the atmospheres of Titan, Triton, and Pluto.[2−4] In a previous publication we characterized the three 3p Rydberg states of diazomethane by using resonance enhanced multiphoton ionization (REMPI) spectroscopy, photoelectron velocity map imaging (VMI) and high-level electronic structure calculations.[5] Emphasis was placed on the effect of electronic-state interactions on the spectroscopy, and both Rydberg−Rydberg and Rydberg−valence interactions were identified and analyzed. The two main resonant structures of ground-state diazomethane are shown in Figure 1. Both structures are ionic and have positively charged central nitrogen, with the negative charge localized on either the terminal nitrogen or the carbon atom. The two structures differ by the hybridization of the carbon: sp^2 versus sp^3.

The present work is centered on the characterization of the normal modes of the 3p Rydberg states of diazomethane and its isotopologs. By comparing the normal-mode frequencies of the 3p Rydberg states to those of the ground state of the neutral (1^1A_1) and the cation (1^2B_1), we analyze the influence of the unpaired electron in each of the 3p orbitals on the structure and vibrational motions in the Rydberg states.

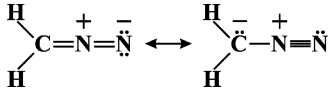

Figure 1. Two Lewis structures for diazomethane. The *z*-axis is along CNN, the *y*-axis is in the plane, perpendicular to CNN, and the *x*-axis is out of plane.

The strategy adopted in this work is the following. Using high level theory we calculate the normal mode harmonic frequencies of the target states for CH_2N_2, CD_2N_2, and $CHDN_2$, and compare them to available experimental results. Some experimental frequencies for the neutral and ion ground states and the $2^1B_1(3p_z)$ Rydberg state are available in the literature,[6−17] and we complement those with new experimental data on the normal modes of the $2^1A_2(3p_y)$ Rydberg state and the ground-state cation. In our previous work,[5] 2 + 1 REMPI spectra and photoelectron VMI of the excited states of CH_2N_2 have been used for the first time to characterize the spectrum of diazomethane in a molecular beam, and these studies are extended here to the isotopologs of diazomethane and to higher excitation

* Corresponding authors. E-mail: reisler@usc.edu (H.R.), krylov@usc.edu (A.I.K.).

10.1021/jp0768064 CCC: $37.00 © 2007 American Chemical Society
Published on Web 12/06/2007

energies (51 750−58 500 cm^{-1}). The excellent agreement between theory and experiment allows us to present a full discussion of the influence of the 3p Rydberg electron on the vibrational frequencies of the corresponding excited states as compared to those of the ground states of the neutral and the cation.

In the 2 + 1 REMPI spectrum of the $2^1A_2 \leftarrow 1^1A_1(3p_y \leftarrow \pi)$ transition of CH_2N_2 obtained before,[5] strong *K*-resolved transitions not seen in one-photon absorption[16] were observed. Using a combination of experiment and theory, the upper states of the observed transitions were assigned, in order of increasing energy, to the $2^1A_2(3p_y \leftarrow \pi)$, $2^1B_1(3p_z \leftarrow \pi)$, and $3^1A_1(3p_x \leftarrow \pi)$ Rydberg states. Although the out-of-plane $3p_x$ Rydberg orbital is usually the least perturbed by the molecular core, the spectrum associated with this state is found to be more perturbed than those associated with the $3p_y$ and $3p_z$ states whose unpaired electrons occupy in-plane orbitals. The 2 + 1 REMPI signal for the $3^1A_1(3p_x \leftarrow \pi)$ state is broader and several times lower in peak intensity than that for transitions to the $2^1A_2(3p_y)$ or $2^1B_1(3p_z)$ states. This broadening is shown by ab initio calculations to result from mixing of the $3^1A_1(3p_x)$ Rydberg state with the dissociative valence $2^1A_1(\pi^* \leftarrow \pi)$ state,[5] which shortens the lifetime of this state and reduced its ionization efficiency. Also, the geometry of the $3^1A_1(3p_x)$ state is quite different from the cation (C_{2v}) having C_s symmetry,[5] in contrast to the $2^1A_2(3p_y)$ and $2^1B_1(3p_z)$ states, which like the cation have C_{2v} symmetry.

In addition, analyses of photoelectron kinetic energy (eKE) distributions of CH_2N_2 indicate that the band origin of the $2^1B_1(3p_z)$ state is mixed with the $2^1A_2(3p_y)$ ν_9 level, which is of B_1 vibronic symmetry.[5] However, most of the other bands in its 2 + 1 REMPI spectrum can be assigned as pure transitions to the $2^1A_2(3p_y)$ state.

The paper is organized as follows. In section 2 we describe the 2 + 1 REMPI and VMI techniques used here and the procedures employed for recording REMPI and photoelectron spectra. Section 3 presents experimental results for the three isotopologs of diazomethane, and describes rotational analyses, the assignment of the band origins of the transitions to the $2^1A_2(3p_y)$ and $2^1B_1(3p_z)$ states, and the mixings of vibronic levels of these Rydberg states. Section 4 describes the electronic structure models, and the results of calculations of geometries and vibrational frequencies of the neutral and cation ground states and the three 3p Rydberg states for the isotopologs of diazomethane. In section 5, after discussing the proposed assignments, we present a detailed analysis of the structure and normal-mode frequencies of Rydberg states of diazomethane and their dependence on the Rydberg electron. The main results and conclusions are summarized in Section 6.

2. Experimental Details

The experimental setup, techniques, and CH_2N_2 synthesis have been described in detail elsewhere,[5,18,19] and only changes and modifications are elaborated upon here. The method used to produce CD_2N_2 and $CHDN_2$ is based on the earlier one for production of CH_2N_2. This method for simultaneously producing CH_2N_2, CD_2N_2, and $CHDN_2$ has the advantage that isotopologs can be prepared using protonated precursors and solvents, and only the aqueous NaOD in D_2O needs to be deuterated. The same glass vacuum line was used for the synthesis.[5] In the modified procedure, CH_2N_2, CD_2N_2, and $CHDN_2$ were generated under vacuum in a closed reactor by the reaction of 2.6 g of *N*-methyl-*N*′-nitro-*N*-nitrosoguanidine (TCI America) dissolved in 30 mL of tetrakis(ethylene glycol) dimethyl ether, 99% (Aldrich) with an excess of ∼7.5 mL aqueous solution of NaOD (2.5M) and 7.5 mL of NaOH (2.5M) mixture. When only ∼15 mL of aqueous NaOD (2.5 M) solution is used, CD_2N_2 in isotopic purity of up to 94% and high overall yield[20] is prepared. The solution was stirred for ∼10 min at 0 °C (273 K) and expanded through two traps held at −78 °C (195 K) with a dry ice/ethanol slush in an 12 L glass flask that was evacuated, protected from exposure to light, and housed in a steel mesh box. A mixture of approximately 0.5% CH_2N_2, 0.5% CD_2N_2, and 0.5% $CHDN_2$ in He at 2 atm total pressure was prepared in this flask. This mixture was introduced into the source chamber of the differentially pumped vacuum system.

The IR and UV spectra of CH_2N_2, CD_2N_2, and $CHDN_2$ prepared by this procedure were in good agreement with published spectra[6−9,21,22] and contained negligible amounts of impurities. On the basis of the IR spectra, samples of CH_2N_2:CD_2N_2:$CHDN_2$ ∼ 1:1:1 are generated; they survive for several days until depleted by use.

2 + 1 REMPI spectra of CH_2N_2, CD_2N_2, and $CHDN_2$ were recorded simultaneously by integrating parent ion peaks of m/e = 42, 44, and 43, respectively, as a function of laser excitation wavelength. The UV laser radiation (0.4−1.1 mJ focused by a 45 cm focal length lens) was generated by frequency doubling (Inrad Autotracker III) the linearly polarized output of a Nd:YAG (Spectra Physics GCR230) pumped dye laser system (Continuum ND6000, LDS 751 and LDS 698, 25−35 mJ). No attempt was made to normalize the spectrum.

Using VMI,[23] we recorded photoelectron images at wavelengths corresponding to state-selected rovibronic levels in the excited 3p Rydberg states, as described before.[5,18,19] For energy calibration, NO ionization via the $A^2\Sigma^+$ state was used.[19] The peaks in the photoelectron kinetic energy (eKE) distributions allowed us to determine vibrational frequencies in the resulting cation. The photoelectrons were extracted and accelerated by the ion optics toward the MCP detector. Signals from the detector were monitored with a CCD camera, transferred to a PC and accumulated. The eKE distributions were determined from the recorded images, by using event counting and centroiding[24,25] and the basis set expansion (BASEX) Abel transform method.[26]

Caution! We wish to emphasize that CH_2N_2 is a toxic, hazardous, and potentially explosive gas, which can decompose violently and spontaneously, and thus appropriate safety precautions must be taken. CH_2N_2 should be handled only at low pressures and on a small scale, and at no time should the gas be allowed to condense into the liquid phase. The pressure must be kept at <25 Torr. Safety equipment (blast shields, safety glasses, face shields, leather gloves, and protective clothing such as leather suits, Kevlar sleeves, and earplugs) must be used, and care must be taken to avoid known triggers of CH_2N_2 decomposition such as intense light, exposure to rough, metallic, or acidic surfaces, and abrupt changes in temperature, pressure, or phase.

3. Experimental Results and Analysis

3.1. REMPI Spectra and eKE Distributions. Figure 2 displays the 2 + 1 REMPI spectra of (a) CH_2N_2, (b) CD_2N_2, and (c) $CHDN_2$ obtained by recording parent ion masses of m/e = 42, 44, and 43, respectively, as a function of 2-photon laser excitation from 51 750 to 54 900 cm^{-1}. Figure 2a also includes an inset of the 54 900 to 56 700 cm^{-1} spectrum that shows the CH stretch region. The observed band positions together with the proposed assignments are listed in Tables 1−3 (see also section 5).

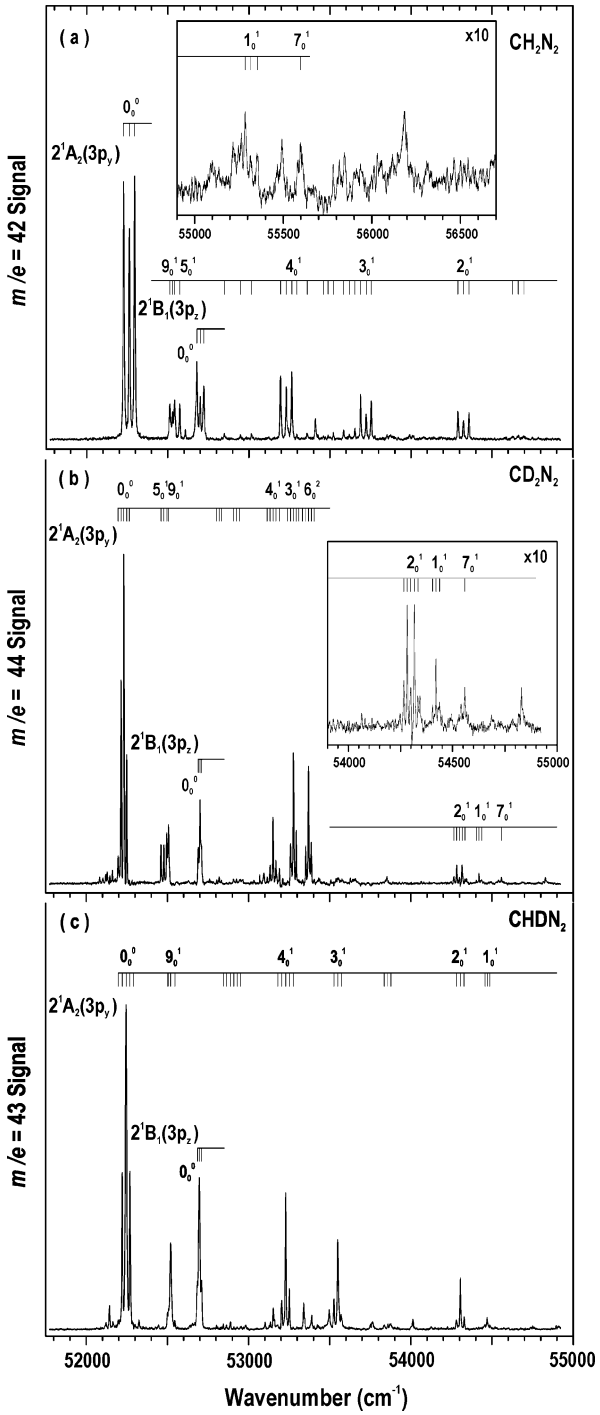

Figure 2. 2 + 1 REMPI spectra for for (a) CH_2N_2, (b) CD_2N_2, and (c) $CHDN_2$ following two-photon laser excitation at 51 750−54 900 cm^{-1}. An inset in (a) for CH_2N_2 shows a 54 900−56 700 cm^{-1} spectrum magnified ten times, whereas an inset in (b) diplays the 54 500−55 000 cm^{-1} range in x10 maginification.

Bands characterized as pure vibronic transitions are assigned by their positions in the 2 + 1 REMPI spectra and the corresponding eKE distributions obtained by VMI. The latter typically have a single, narrow band corresponding to the diagonal transition between the vibronic level in the Rydberg state and the corresponding vibrational level of the cation. An example is shown in Figure 3, which displays the eKE distribution for CD_2N_2 obtained at excitation wavelength λ = 381.14 nm ($2h\nu$ = 52 478 cm^{-1}), and which has one strong, narrow band at 5857 cm^{-1} assigned as ν_5^+ (see section 5). Most of the vibronic bands of the three isotopologs of diazomethane exhibit similar single peaks in their eKE distributions.

Mixed levels involving the band origin of the $2^1B_1(3p_z)$ Rydberg state and the ν_9 level of the $2^1A_2(3p_y)$ Rydberg state in CD_2N_2 and $CHDN_2$ were characterized as described before for CH_2N_2.[5] Briefly, the eKE distributions of CD_2N_2 and $CHDN_2$ bands were similar in shape to those of CH_2N_2 at spectral positions where the mixed levels were expected,[5] and Figures 4 and 5 show representative examples. The distributions for CD_2N_2 obtained at λ = 380.93 nm (52 507 cm^{-1}) and at λ = 379.51 nm (52 700 cm^{-1}) are similar to one another (Figure 4). Each has two prominent, narrow bands (at 5799 and 6136 cm^{-1} and at 6089 and 6429 cm^{-1} in Figure 4a,b, respectively) separated by ∼340 ± 20 cm^{-1}. The eKE distribution in Figure 4b has an additional peak (at 5514 cm^{-1}), which does not appear in Figure 4a. In the case of $CHDN_2$, the images and the corresponding eKE distributions depicted in Figure 5a (λ = 380.81 nm (52 520 cm^{-1})) and 5b (λ = 379.53 nm (52 697 cm^{-1})) are similar to those shown in Figure 4. The separation between the two most intense bands (at 5807 and 6182 cm^{-1} and at 6078 and 6453 cm^{-1} in Figure 5a,b, respectively) is ∼375 ± 20 cm^{-1}. The eKE distribution in Figure 5b has additional peaks at 5493 cm^{-1} and 5157 cm^{-1}. Similar to CH_2N_2,[5] the strong outermost ring in the CD_2N_2 and $CHDN_2$ images has an anisotropic angular distribution, whereas the strong inner rings are isotropic. The relative width of the peaks is $\Delta E/E$ = 3.0 ± 0.2%, close to the instrument resolution.

3.2. Spectroscopic Analysis: Band Origins, *K*-Structure, and State Interactions. CH_2N_2, CD_2N_2, and $CHDN_2$ in their neutral ground states are near-symmetric prolate tops.[6,27,28] According to electronic structure calculations, the $3p_y$ and $3p_z$ Rydberg states as well as the ground-state cation are planar, similarly to the neutral ground state. Thus, in accordance with the Franck−Condon principle, the origin bands in the 2 + 1 REMPI spectrum and bands associated with the totally symmetric vibrational (a_1) levels should have the highest intensities, as indeed observed.

The *K*-structure can aid in assigning the symmetry of the transitions. For CH_2N_2 and CD_2N_2, vibronic transitions from the vibrational ground state to vibronic bands of A_1 and A_2 symmetry are governed by $\Delta K = 0, \pm 2$ selection rules with a 4A′ spacing between *K* bands, whereas transitions to B_1 and B_2 vibronic bands are governed by a $\Delta K = \pm 1$ selection rule with a 2A′ spacing.[29] The electronic wavefunctions of the $3p_y$ and $3p_z$ Rydberg states of $CHDN_2$ have C_{2v} symmetry and, therefore, follow the same selecton rules.

For CH_2N_2 we found before that all the observed transitions originate from $K'' = 0$ and 1, and those originating from $K'' = 1$ are the most intense, in accordance with nuclear spin statistics.[5] Because of the smaller rotational constants of CD_2N_2 and $CHDN_2$, rotational bands originating from $K'' = 2$ are also observed. For CD_2N_2, rotational transitions from $K'' = 0$ and 2 have twice the intensity of those from $K'' = 1$ because of nuclear spin statistics. These intensity patterns explain the differences in relative intensities of vibronic bands associated with different *K* transitions, and we use them, whenever possible, in assigning the vibronic transitions (see section 5).

In experiments employing VMI,[5,18,19,23] the internal energy (E_{int}) of the ion corresponding to each measured photoelectron peak is calculated from the peak position in the eKE distribution:

$$E_{int} = 3h\nu - e\mathrm{KE} - \mathrm{IE} \qquad (1)$$

where the adiabatic ionization energy IE was taken as the published value for CH_2N_2 (9.00 ± 0.02 eV; 72 585 ± 160

TABLE 1: Transition Energies and Vibrational Assignments[a] for the $2^1A_2(3p_y) \leftarrow 1^1A_1$ Transition of CH_2N_2[b]

two-photon energies	ΔE[c]	intensity	assignments	$K' \leftarrow K''$
52227	0		0_0^0	$0 \leftarrow 0, 1 \leftarrow 1$
52262	35	strong	0_0^0	$2 \leftarrow 0$
52295	68		0_0^0	$3 \leftarrow 1$
52513 (52575)[d]	286 (348)		9_0^1	$0 \leftarrow 1$
52528 (52590)	301 (363)	strong	9_0^1	$1 \leftarrow 0$
52541 (52603)	314 (376)		9_0^1	$2 \leftarrow 1$
52574	347	strong	5_0^1	
52850	623	weak	(6_0^1)	
52947	720	weak	$(5_0^2;6_0^1;9_0^2)$	
53016	789	weak	$(5_0^2;6_0^1;9_0^2)$	
53196	969		4_0^1	$0 \leftarrow 0, 1 \leftarrow 1$
53230	1003	strong	4_0^1	$2 \leftarrow 0$
53265	1038		4_0^1	$3 \leftarrow 1$
53296	1069	weak	(9_0^3)	
53359	1132	weak	(5_0^3)	
53459	1232		$5_0^1 6_0^1$	
53489	1262	weak	$5_0^1 6_0^1$	
53522	1295		$5_0^1 6_0^1$	
53585	1358		(6_0^2)	
53619	1392	medium	(6_0^2)	
53654	1427		(6_0^2)	
53690	1463		3_0^1	$0 \leftarrow 0, 1 \leftarrow 1$
53723	1496	strong	3_0^1	$2 \leftarrow 0$
53756	1529		3_0^1	$3 \leftarrow 1$
54289	2062		2_0^1	$0 \leftarrow 0, 1 \leftarrow 1$
54324	2097	strong	2_0^1	$2 \leftarrow 0$
54358	2131		2_0^1	$3 \leftarrow 1$
54627	2400		$3_0^1 4_0^1$	
54662	2435	weak	$3_0^1 4_0^1$	
54697	2470		$3_0^1 4_0^1$	
54986	2759		$2_0^1 6_0^1$	
55006	2779	weak	$2_0^1 6_0^1$	
55027	2800		$2_0^1 6_0^1$	
55286	3059		1_0^1	$0 \leftarrow 0, 1 \leftarrow 1$
55318	3091	weak	1_0^1	$2 \leftarrow 0$
55353	3126		1_0^1	$3 \leftarrow 1$
55597	3370	weak	7_0^1	

[a] Where known, the K assignment is also given. Tentatively assigned frequencies are enclosed in parentheses. [b] All values in cm^{-1} (uncertainty $\pm$ 5 cm^{-1}). [c] ΔE are energies of transitions determined with respect to the band origin. [d] Deperturbed band positions are shown in parentheses.

cm^{-1}).[17] This value was confirmed by our photoelectron spectra, and was the same, within the error bar, for all isotopologs (see below).

The 2 + 1 REMPI spectrum of CH_2N_2 in the 51 750−56 700 cm^{-1} energy region is shown in Figure 2a, and transitions in the 52 227−52 722 cm^{-1} region have been assigned before.[5] The most intense group of bands, at 52 227−52 295 cm^{-1}, belongs to the origin band of the $2^1A_2 \leftarrow 1^1A_1$ ($3p_y \leftarrow \pi$) transition. The three components of this band, which are spaced by ~4A″, correspond to K rotational structure (see Table 1).

The strong bands with partially resolved rotational structure at 52 513−52 541 and 52 679−52 722 cm^{-1} were assigned before as mixed bands composed of the 9_0^1 transition to the $2^1A_2(3p_y)$ state and the band origin of the $2^1B_1 \leftarrow 1^1A_1$ ($3p_z \leftarrow \pi$) transition.[5] These bands were deperturbed by using a two-level approximation. The deperturbed origin band of the $2^1B_1 \leftarrow 1^1A_1$ ($3p_y \leftarrow \pi$) transition was determined at 52 638 cm^{-1} and the coupling matrix element was found to be 83 cm^{-1}.[5]

The 2 + 1 REMPI spectra of CD_2N_2 and $CHDN_2$ in the 51 750−54 900 cm^{-1} energy region are shown in Figure 2b,c, respectively, and the band assignments follow those for CH_2N_2. For CD_2N_2, the origin band of the $2^1A_2 \leftarrow 1^1A_1$ ($3p_y \leftarrow \pi$) transition is at 52 196−52 266 cm^{-1}. The five components of this band, which are spaced by ~4A″, correspond to the K rotational structure. The lower energy peak arises from the $K' = 0 \leftarrow K'' = 2$ transitions. The next one arises mostly from the $K' = 0 \leftarrow K'' = 0$ and $K' = 1 \leftarrow K'' = 1$ transitions with some contribution from $K' = 2 \leftarrow K'' = 2$. The most intense peak corresponds to the $K' = 2 \leftarrow K'' = 0$ transition, and the last two peaks are from the $K' = 3 \leftarrow K'' = 1$ and $K' = 4 \leftarrow K'' = 2$ transitions, respectively.

Analyses of the two-peak structures in the eKE distributions for CD_2N_2 obtained at λ = 380.93 nm (52 507 cm^{-1}) and at λ = 379.51 nm (52 700 cm^{-1}) (Figure 4) show that the mixing of the $2^1A_2(3p_y)$ 9_0^1 transition and the band origin of $2^1B_1 \leftarrow 1^1A_1$ ($3p_z \leftarrow \pi$) is only slightly weaker than in CH_2N_2. This is because the ν_9' mode (CNN in-plane bend) does not involve distortion of the CH_2 group and therefore the mixing does not change significantly with H/D substitution. A deperturbation analysis (using a two-level approximation) places the 2^1B_1 origin of CD_2N_2 at 52 664 cm^{-1} with a coupling matrix element of 71 cm^{-1}.

The peaks in the eKE distributions shown in Figure 4b correspond to vibrational levels ν_0^+ and ν_9^+ (340 ± 20 cm^{-1}) of the cation. The peaks in the eKE distributions obtained at 52 495 cm^{-1} and 52 507 cm^{-1} (Figure 4a) have similar relative intensities and peak separations (340 ± 20 cm^{-1}). The peak at

TABLE 2: Transition Energies and Vibrational Assignments[a] for the $2^1A_2(3p_y) \leftarrow 1^1A_1$ Transition of CD_2N_2[b]

two-photon energies	ΔE[c]	intensity	assignments	$K' \leftarrow K''$
52196	−18		0_0^0	$0 \leftarrow 2$
52214	0		0_0^0	$0 \leftarrow 0, 1 \leftarrow 1, 2 \leftarrow 2$
52231	17	strong	0_0^0	$2 \leftarrow 0$
52249	35		0_0^0	$3 \leftarrow 1$
52266	52		0_0^0	$4 \leftarrow 2$
52461	247		5_0^1	
52478	264	strong	5_0^1	
52495 (52526)[d]	281 (312)		9_0^1	$0 \leftarrow 1$
52507 (52538)	293 (324)	strong	9_0^1	$1 \leftarrow 0$
52804	590		(6_0^1)	
52818	604	medium	(6_0^1)	
52832	618		(6_0^1)	
52908	694		9_0^2	
52925	711	weak	9_0^2	
52943	729		9_0^2	
53115	901		4_0^1	$0 \leftarrow 2$
53133	919		4_0^1	$0 \leftarrow 0, 1 \leftarrow 1, 2 \leftarrow 2$
53150	936	strong	4_0^1	$2 \leftarrow 0$
53168	954		4_0^1	$3 \leftarrow 1$
53191	977		4_0^1	$4 \leftarrow 2$
53241	1027		3_0^1	$0 \leftarrow 2$
53258	1044		3_0^1	$0 \leftarrow 0, 1 \leftarrow 1, 2 \leftarrow 2$
53276	1062	strong	3_0^1	$2 \leftarrow 0$
53293	1079		3_0^1	$3 \leftarrow 1$
53310	1096		3_0^1	$4 \leftarrow 2$
53334	1120		6_0^2	$0 \leftarrow 2$
53352	1138		6_0^2	$0 \leftarrow 0, 1 \leftarrow 1, 2 \leftarrow 2$
53369	1155	strong	6_0^2	$2 \leftarrow 0$
53386	1172		6_0^2	$3 \leftarrow 1$
53404	1190		6_0^2	$4 \leftarrow 2$
54265	2051	medium	2_0^1	$0 \leftarrow 0, 1 \leftarrow 1, 2 \leftarrow 2$
54282	2068		2_0^1	$2 \leftarrow 0$
54299	2085		2_0^1	$3 \leftarrow 1$
54316	2102	medium	3_0^2	$2 \leftarrow 0$
54333	2119		3_0^2	$3 \leftarrow 1$
54403	2189		1_0^1	$0 \leftarrow 0, 1 \leftarrow 1, 2 \leftarrow 2$
54420	2206	medium	1_0^1	$2 \leftarrow 0$
54437	2223		1_0^1	$3 \leftarrow 1$
54558	2344	weak	7_0^1	

[a] Where known, the K assignment is also given. Tentatively assigned frequencies are enclosed in parentheses. [b] All values in cm^{-1} (uncertaity $\pm$ 5 cm^{-1}). [c] ΔE are energies of transitions determined with respect to the band origin. [d] Deperturbed band positions are shown in parentheses.

5514 cm^{-1} in Figure 4b is assigned to the ν_4^+ mode (915 $\pm$ 20 cm^{-1}). The three peaks in the REMPI spectrum at 52 690−52 710 cm^{-1} are assigned, in order of increasing energy, to the $K' = 0 \leftarrow K'' = 1$, $K' = 1 \leftarrow K'' = 0$, and $K' = 2 \leftarrow K'' = 1$ transitions, respectively. No transitions from $K'' = 2$ were detected.

For $CHDN_2$ the origin band of the $2^1A_2 \leftarrow 1^1A_1$ ($3p_y \leftarrow \pi$) transition is at 52 197−52 291 cm^{-1} and similarly to CD_2N_2, transitions originating from $K'' = 2$ were observed. The spacing between the five components of the K rotational structure is $\sim 4A''$ and the proposed K assignments are given in Table 3.

The eKE distributions for $CHDN_2$ obtained at $\lambda = 380.81$ nm (52 520 cm^{-1}) and $\lambda = 379.53$ nm (52 697 cm^{-1}) (Figure 5) are similar to those shown in Figure 4. Analysis of the structure in the eKE distributions indicates that the interaction between the $2^1A_2(3p_y)$ 9_0^1 transition and the band origin of the $2^1B_1 \leftarrow 1^1A_1$ ($3p_z \leftarrow \pi$) transition is of intermediate strength between CH_2N_2 and CD_2N_2. A deperturbation analysis (using a two-level approximation) places the 2^1B_1 origin at 52 648 cm^{-1} with a coupling matrix element of 76 cm^{-1}.

The peaks in the eKE distributions shown in Figure 5 correspond to vibrational levels ν_0^+ and ν_9^+ (375 $\pm$ 20 cm^{-1}). The peaks at 5493 cm^{-1} and 5157 cm^{-1} in Figure 5b are assigned to ν_4^+ and $\nu_4^+ + \nu_9^+$ (where ν_9^+ is the CNN in-plane bend and ν_4^+ is the CN stretch) in the $CHDN_2^+$ ion, which have frequencies $\sim$960 $\pm$ 20 and 1296 $\pm$ 30 cm^{-1}, respectively. The three peaks in the REMPI spectrum at 52 684−52 710 cm^{-1} are assigned, in order of increasing energy, to the $K' = 0 \leftarrow K'' = 1$, $K' = 1 \leftarrow K'' = 0$, and $K' = 2 \leftarrow K'' = 1$ transitions to the perturbed 2^1B_1 ($3p_z \leftarrow \pi$) state, respectively. No transitions originating from $K'' = 2$ were detected for this state.

4. Theoretical Methods and Results

The equilibrium geometry and vibrational frequencies of neutral diazomethane were calculated by CCSD(T)[30,31]/cc-pVTZ[32] and B3LYP[33]/6-311G(2df,p). Geometry and frequencies of the ground state of the cation were calculated by CCSD(T)/cc-pVTZ using the unrestricted (UHF) reference. The basis sets were derived from the polarized split-valence 6-311G(d,p) basis by adding additional polarization and diffuse functions.[34,35]

Isotope shifts for the ground-state neutral and the cation were calculated at the B3LYP/6-311G(2df,p) level. The equilibrium structures, frequencies, and isotope shifts of the $2^1A_2(3p_y)$ and

TABLE 3: Transition Energies and Vibrational Assignments[a] for the $2^1A_2(3p_y) \leftarrow 1^1A_1$ Transition of $CHDN_2$[b]

two-photon energies	ΔE[c]	intensity	assignments	$K' \leftarrow K''$
52197	−24		0_0^0	$0 \leftarrow 2$
52221	0		0_0^0	$0 \leftarrow 0, 1 \leftarrow 1, 2 \leftarrow 2$
52245	24	strong	0_0^0	$2 \leftarrow 0$
52268	47		0_0^0	$3 \leftarrow 1$
52291	70		0_0^0	$4 \leftarrow 2$
52500 (52543)[d]	279 (322)		9_0^1	
52507 (52550)	286 (329)	strong	9_0^1	
52520 (52563)	299 (342)		9_0^1	
52546 (52589)	325 (368)		9_0^1	
52845	624		(6_0^1)	
52865	644	weak	(6_0^1)	
52887	666		(6_0^1)	
52910	689		9_0^2	
52931	710	weak	9_0^2	
52953	732		9_0^2	
53180	959		4_0^1	$0 \leftarrow 2$
53204	983		4_0^1	$0 \leftarrow 0, 1 \leftarrow 1, 2 \leftarrow 2$
53229	1008	strong	4_0^1	$2 \leftarrow 0$
53251	1030		4_0^1	$3 \leftarrow 1$
53275	1054		4_0^1	$4 \leftarrow 2$
53526	1305		3_0^1	$0 \leftarrow 0, 1 \leftarrow 1, 2 \leftarrow 2$
53549	1328	strong	3_0^1	$2 \leftarrow 0$
53570	1349		3_0^1	$3 \leftarrow 1$
53835	1614		$(3_0^1 9_0^1)$	
53858	1637	weak	$(3_0^1 9_0^1)$	
53878	1657		$(3_0^1 9_0^1)$	
54281	2060		2_0^1	$0 \leftarrow 0, 1 \leftarrow 1, 2 \leftarrow 2$
54305	2084	strong	2_0^1	$2 \leftarrow 0$
54328	2107		2_0^1	$3 \leftarrow 1$
54458	2237		1_0^1	$0 \leftarrow 0, 1 \leftarrow 1, 2 \leftarrow 2$
54472	2251	medium	1_0^1	$2 \leftarrow 0$
54487	2266		1_0^1	$3 \leftarrow 1$
55197	2976	weak	7_0^1	

[a] Where known, the *K* assignment is also given. Tentatively assigned frequencies are enclosed in parentheses. [b] All values in cm^{-1} (uncertainty $\pm$ 5 cm^{-1}). [c] ΔE are energies of transitions determined with respect to the band origin. [d] Deperturbed band positions are shown in parentheses.

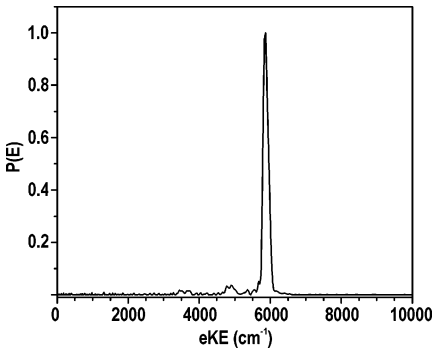

Figure 3. eKE distribution for CD_2N_2 obtained from the photoelectron image at excitation wavelength $\lambda = 381.14$ nm ($2h\nu = 52\,478$ cm^{-1}).

$2^1B_1(3p_z)$ Rydberg states were calculated by EOM-EE-CCSD[36−38] with 6-311(3+,+)G(2df). Although equilibrium structures, excitation energies, and most of the skeletal frequencies are reasonably converged with just a single polarization set, additional polarization functions are crucial for out-of-plane vibrations, probably due to rehybridization induced by those motions. For instance, the CH_2 wagging frequency in the $2^1A_2(3p_y)$ and $2^1B_1(3p_z)$ states increases by 93 and 74 cm^{-1}, respectively, upon increasing polarization from 6-311(3+,+)G(d) to 6-311(3+,+)G(2df). A smaller 6-31(2+)G(d) basis was employed for the (lower-symmetry) $3^1A_1(3p_x)$ state to reduce computational costs.

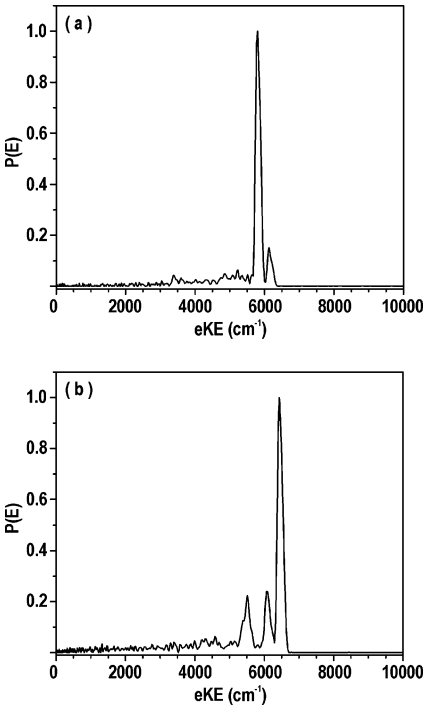

Figure 4. eKE distributions for CD_2N_2 obtained from photoelectron images at excitation wavelength (a) $\lambda = 380.93$ nm (52 507 cm^{-1}) and (b) $\lambda = 379.51$ nm ($2h\nu = 52\,700$ cm^{-1}).

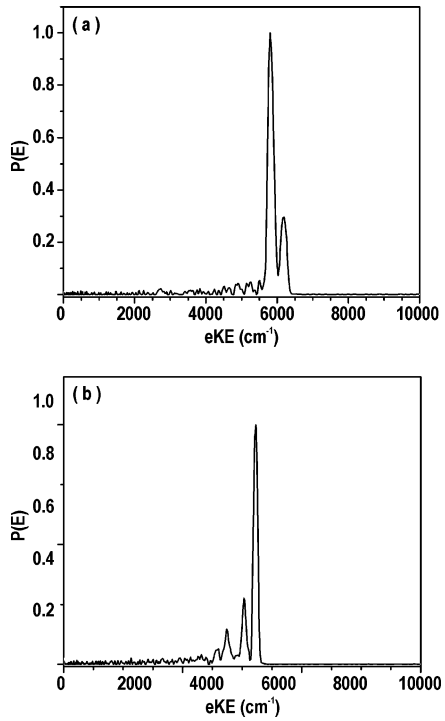

Figure 5. eKE distributions for $CHDN_2$ obtained from photoelectron images at excitation wavelength (a) $\lambda = 380.81$ nm (52 520 cm^{-1}) and (b) $\lambda = 379.53$ nm (52 697 cm^{-1}).

Vertical excitation energies and adiabatic IE's were calculated using EOM-CCSD/6-311(3+,+)G(d) and EOM-IP-CCSD[39−41]/6-311G(2df,p), respectively, at the B3LYP/6-311G(2df, p) optimized geometries.

All optimizations, frequencies, and excited-state calculations were performed using the Q-Chem[42] and ACES II[43] electronic structure programs. The natural bond orbital (NBO) program[44] was employed to analyze bonding in neutral, electronically excited and ionized diazomethane.

All equilibrium geometries are summarized in Table 4. Note that within the Born−Oppenheimer approximation, the equilibrium geometries of all isotopologs are identical. Moreover, because the symmetry of the nuclear Coulomb potential is also the same, the C_{2v} point group may be used for the electronic wave functions in all cases.

Tables 5−7 present calculated (harmonic) and experimental (fundamental) vibrational frequencies for CH_2N_2, CD_2N_2, and $CHDN_2$, respectively. The B3LYP and CCSD(T) results for the neutral are in good agreement, which validates the B3LYP results for isotope shifts. The comparison between the theoretical and experimental results, as well as the changes in structures and frequencies induced by ionization and electronic excitation are discussed in Section 5.

5. Discussion

5.1. Vibrational Assignments for the $2^1A_2(3p_y)$ Rydberg State. As stated above, one of the goals of the present work is to determine experimentally the fundamental vibrational modes of the $2^1A_2(3p_y)$ state of diazomethane and its cation to compare them with theoretical calculations. In the REMPI spectra, the strongest transitions to the Rydberg $2^1A_2(3p_y)$ state are those of a_1 vibrational symmetry and their assignments are robust. Bands of b_1 and b_2 symmetry are much weaker and often do not show a discernible *K*-structure. Their assignments, which rely mainly on calculations, are tentative. The proposed assignments for CH_2N_2, CD_2N_2, and $CHDN_2$ are shown in Figure 2a−c and the fundamental frequencies are listed in Tables 5−7.

In assigning fundamental frequencies in the $2^1A_2(3p_y)$ state we relied on (i) the measured positions of the REMPI vibronic bands, (ii) the *K*-structure of the vibronic bands, (iii) the energy positions of the diagonal peaks in the eKE distributions, (iv) changes observed for H/D isotopologs, and (v) results of ab initio calculations. The observed eKE distributions of all the unperturbed peaks appeared isotropic.

As discussed previously,[5] 2 + 1 REMPI excites mostly vibronic levels in the $2^1A_2(3p_y)$ state, and transitions of a_1 symmetry to $\nu'_1-\nu'_4$ exhibit the highest intensity. For example, in the 2 + 1 REMPI spectrum of CH_2N_2 (Figure 2a), the strong bands at 53 196−53 265, 53 690−53 756, 54 289−54 358, and 55 286−55 353 cm^{-1} are assigned, respectively, as the 4_0^1, 3_0^1, 2_0^1, and 1_0^1 transitions to the $2^1A_2(3p_y \leftarrow \pi)$ state. The corresponding frequencies of the totally symmetric (a_1) ν'_4, ν'_3, ν'_2, and ν'_1 fundamentals are 969, 1463, 2062, and 3059 cm^{-1}, respectively, in good agreement with the calculated values (Table 5). These assignments are confirmed by the positions of combination bands at 54 627−54 679 and 55 783−55 846 cm^{-1}, which are assigned as $3_0^1\,4_0^1$ and $2_0^1\,3_0^1$, respectively. CD_2N_2 and $CHDN_2$ transitions involving the totally symmetric modes are also intense, and it is easy to identify the 4_0^1, 3_0^1, 2_0^1, and 1_0^1 transitions. For CD_2N_2 (Figure 2b), the frequencies of ν'_4, ν'_3, ν'_2, and ν'_1 are 919, 1044, 2051, and 2189 cm^{-1}, respectively, and for $CHDN_2$ (Figure 2b), they are 983, 1305, 2060, and 2237 cm^{-1}.

A further test of the reliability of the assignments is that bands involving CH or CD motions change their frequency as expected for isotopic substitution. For example, the CH and CD stretch fundamentals in $CHDN_2$ have a frequency ratio CH:CD ∼ 1.4. All the experimentally determined values of the fundamental vibrational frequencies of a_1 symmetry are in good agreement with the calculated harmonic frequencies (Tables 5−7).

Whereas it is fairly easy to assign the totally symmetric fundamentals, this is not the case for the weak bands of b_1 and b_2 symmetry. The transitions to the $\nu_9(b_2)$ fundamentals are mixed with the 2^1B_1 origin bands, and this mixing lends them intensity. The unperturbed energies of the upper states were determined by using a two-state approximation, as described before, and these values are listed in the tables.

In our previous paper we assigned the strong band of CH_2N_2 located at 52 574 cm^{-1} as the 5_0^1 transition to $2^1A_2(3p_y)$.[5] The separation between the triad of bands in CD_2N_2 at 52 461−52 495 cm^{-1} is ∼17 cm^{-1}, which is typical of transitions of A_1 or A_2 rovibronic levels. However, these bands could not be assigned to any of the a_1 modes or their combinations. They are closest to the calculated frequency of the 5_0^1 transition, resulting in a ν'_5 (b_1; CNN out-of-plane bend) frequency of 264 cm^{-1}. The single peak in the corresponding eKE distribution, whose frequency is 275 ± 10 cm^{-1} is assigned as ν_5^+. A similar eKE distribution was observed in ionization through the 52 461 cm^{-1} transition for which the internal energy of the cation was calculated to be 225 cm^{-1}. We therefore tentatively assign the upper state of this REMPI transition as ν'_5.

The ν'_6 and ν'_7 normal modes of CH_2N_2, CD_2N_2, and $CHDN_2$, are assigned based primarily on the closeness of observed (weak) REMPI bands to the calculated vibrational frequencies and their isotopic variations. Tentative assignments are shown in parentheses in Tables 1−3 and 5−7. All the assigned fundamental frequencies are summarized and compared with calculations in Tables 5−7.

TABLE 4: Calculated Equilibrium Structures and Nuclear Repulsion Energies for the Ground State of the Neutral and Cation and the 3p Rydberg States of CH_2N_2[a]

	1^1A_1[b]	$3^1A_1(3p_x)$[c]	$2^1A_2(3p_y)$[d]	$2^1B_1(3p_z)$[d]	1^2B_1[e]
E_{nuc} (hartree)	61.514227, 61.280112	59.502297	61.132745	61.137542	61.118198
r_{C-N} (Å)	1.298, 1.292	1.398	1.352	1.343	1.362
r_{N-N} (Å)	1.139, 1.132	1.130	1.105	1.107	1.115
r_{C-H} (Å)	1.071, 1.077	1.084	1.079	1.084	1.086
∠HCH (deg)	125.00, 124.07	128.64	129.96	124.76	127.80
∠NNC (deg)	180, 180	160.55	180	180	180
∠NNHC (deg)	0, 0	92.7	0	0	0

[a] All values remain unchanged for $CHDN_2$ and CD_2N_2. [b] Left values calculated using CCSD(T)/cc-pVTZ; right values, using B3LYP/6-311G(2df, p), respectively. Experimental geometrical values: r_{C-N}, 1.300 Å; r_{N-N}, 1.139 Å; r_{C-H}, 1.077 Å; ∠HCH, 126.1°; ∠NNC, 180°; ∠NNHC, 0°.[28] [c] EOM-CCSD/6-31(2+)G(d). [d] EOM-CCSD/6-311(3+,+)G(2df). [e] CCSD(T)/cc-pVTZ.

TABLE 5: Transitions Energies and Vibrational Frequencies of Neutral Ground State, 3p Rydberg States, and Cation of CH_2N_2[a]

	1^1A_1 exp[b] *calc*[c]	$3^1A_1(3p_x)$ exp[d] *calc*	$2^1A_2(3p_y)$ exp[e] *calc*	$2^1B_1(3p_z)$ exp[f] *calc*	1^2B_1 exp[g] *calc*
band origin, IE		56898	52227	52628	72620, 72585[h]
		77665	*51213*	*51535*	*71375*
$\nu_1(a_1)$ CH_2 sym stretch	3077		3059	2980	3015
	3185, 3230	*3202*	*3182*	*3104*	*3164*
$\nu_2(a_1)$ NN stretch	2102		2062	2142	2110, 2180[h]
	2203, 2173	*2093*	*2225*	*2208*	*2199*
$\nu_3(a_1)$ CH_2 sym bend	1414		1463	1246	1420
	1448, 1462	*1367*	*1424*	*1370*	*1432*
$\nu_4(a_1)$ CN stretch	1170		969	864	985, 970[h]
	1214, 1196	*768*	*1007*	*1007*	*1001*
$\nu_5(b_1)$ CNN o.p. bend	564		347		320
	586, 578	*571*	*448*	*460*	*440*
$\nu_6(b_1)$ CH_2 wag	406		(623)	819	810
	413, 420	*526*	*594*	*767*	*712*
$\nu 7(b_2)$ CH_2 asym stretch	3185		3370		
	3305, 3347	*3368*	*3311*	*3290*	*3311*
$\nu_8(b_2)$ CH_2 rock	1109				
	1125, 1129	*1134*	*1136*	*1088*	*1133*
$\nu_9(b_2)$ CNN i.p. bend	421		356		420
	432, 419	*431*	*352*	*446*	*377*

[a] All values in cm^{-1}; data from this work, unless otherwise stated. Tentatively assigned frequencies are enclosed in parentheses. [b] Data from refs 6 and 7 (frequencies rounded to integer cm^{-1}; accuracy = ±2 cm^{-1}). [c] Harmonic frequencies, see text. For the 1^1A_1 state, the left values calculated using B3LYP/6-311G(2df, p), and the right values by CCSD(T)/cc-pVTZ. For the $3^1A_1(3p_x)$ state, symmetry is lowered to C_s, b_1 modes are of a″ symmetry, and all others are a′. [d] Uncertainty ±15 cm^{-1}. [e] Uncertainty ±5 cm^{-1}. [f] Fundamental frequencies are from ref 16 relative to the determined deperturbed value of the $2^1B_1(3p_z)$ band origin. The perturbed value for the band origin (52 690 cm^{-1}) was defined as the average value for the 1 ← 0 and 0 ← 1 transitions. [g] Frequency accuracy defined as the spacing between the rotational lines of cation is ±50 cm^{-1}. [h] Data from ref 17. Frequency accuracy is ±80 cm^{-1}.

5.2. Vibrational Assignments for the 1^2B_1 Ground-State Cation. The He(II) photoelectron spectrum of diazomethane was reported before,[17] and the adiabatic IE of the ion and the frequencies of several of its vibrational levels were determined (Tables 5 and 6). We obtained these and additional vibrational frequencies from the images by using eq 1. In assigning the ion's vibrational modes and frequencies we used mainly those eKE distributions that had a single peak resulting from the diagonal Franck−Condon transition; i.e., the vibrational frequencies obtained for the excited Rydberg state and the cation were rather similar. As discussed before, in the case of the mixed levels described above, we obtained ionic vibrational frequencies from the peak separations in the eKE distributions.[5] We note that only strong transitions whose signal was high above background could be used reliably because we detect all photoelectrons produced by ionization disregarding of their origin. The eKE for the origin band places the adiabatic IE of the cation at IE = 72 620 ± 100 cm^{-1}, in excellent agreement with the published value of 72 585 ± 160 cm^{-1}.[17] Other isotopologs had the same IE. The uncertainty in our values reflects mainly uncertainty in *K* of about one unit in the ionization step. As with the values for neutral diazomethane, the experimental and theoretical vibrational frequencies for the ions agree very well.

5.3. Structure and Vibrational Motions in Neutral and Ionic Diazomethane. The observed changes in structure and frequencies induced by ionization and electronic excitation (Tables 5−7) can be explained by simple molecular orbital considerations in combination with NBO analysis. As expected from the wave function analysis,[5] the structures and vibrational frequencies of the 2^1A_2 ($3p_y$) and $2^1B_1(3p_z)$ Rydberg states are similar to those of the cation and they both retain C_{2v} structure. The $3^1A_1(3p_x)$ state, however, differs considerably from both the cation and the other two 3p states due to its mixing with the valence 2^1A_1 ($\pi^* \leftarrow \pi$) state, and it has C_s equilibrium structure.[5]

Below we first compare the calculated and experimental values to validate the theoretical results and the assignments, and then proceed to analyze differences in structures and frequencies between the Rydberg states and the cation to understand the structural and spectroscopic signatures of Rydberg−valence, Rydberg−Rydberg, and Rydberg−ion core interactions.

TABLE 6: Transitions Energies and Vibrational Frequencies of Neutral Ground State, 3p Rydberg States, and Cation of CD_2N_2[a]

	1^1A_1 exp[b] *calc*[c]	$3^1A_1(3p_x)$ exp[d] *calc*	$2^1A_2(3p_y)$ exp[e] *calc*	$2^1B_1(3p_z)$ exp[f] *calc*	1^2B_1 exp[g] *calc*
band origin		56871	52214	52664	72620, 72585[h]
$\nu_1(a_1)$ CD_2 sym stretch	2245		2189	2183	
	2305	*2313*	*2302*	*2244*	*2246*
$\nu_2(a_1)$ NN stretch	2096		2051	2081	2180[h]
	2198	*2060*	*2213*	*2197*	*2145*
$\nu_3(a_1)$ CD_2 sym bend	1213		1044	907	
	1267	*1034*	*1076*	*1054*	*1108*
$\nu_4(a_1)$ CN stretch	970		919	766	915, 970[h]
	984	*734*	*949*	*932*	*957*
$\nu_5(b_1)$ CNN o.p. bend			(256)		(225, 275)
	571	*564*	*446*	*444*	*425*
$\nu_6(b_1)$ CD_2 wag	318		(590)	606	
	327	*417*	*457*	*611*	*592*
$\nu_7(b_2)$ CD_2 asym stretch	2414		2344		
	2470	*2527*	*2484*	*2471*	*2440*
$\nu_8(b_2)$ CD_2 rock	903				
	919	*914*	*899*	*891*	*903*
$\nu_9(b_2)$ CNN i.p. bend			(318)		340
	392	*376*	*328*	*401*	*357*

[a] All values in cm^{-1}; data from this work, unless otherwise stated. Tentatively assigned frequencies are enclosed in parentheses. [b] Data from refs 6 and 7 (frequencies rounded to integer cm^{-1}; accuracy = ± 2 cm^{-1}). [c] Harmonic frequencies, see text. For the 1^1A_1 state, the values were calculated using B3LYP/6-311G(2df, p). For the $3^1A_1(3p_x)$ state, symmetry is lowered to C_s, b_1 modes are of a″ symmetry, and all others are a′. [d] Uncertainty ± 15 cm^{-1}. [e] Uncertainty ± 5 cm^{-1}. [f] Fundamental frequencies are from ref 16 relative to the determined deperturbed value of the $2^1B_1(3p_z)$ band origin. The perturbed value for the band origin (52 695 cm^{-1}) was defined as the average value for the $1 \leftarrow 0$ and $0 \leftarrow 1$ transitions. [g] Frequency accuracy defined as the spacing between the rotational lines of cation is ± 50 cm^{-1}. [h] Data from ref 17. Frequency accuracy is ± 80 cm^{-1}.

TABLE 7: Transitions Energies and Vibrational Frequencies of Neutral Ground State, 3p Rydberg States, and Cation of $CHDN_2$[a]

	1^1A_1 exp[b] *calc*[c]	$3^1A_1(3p_x)$ exp[d] *calc*	$2^1A_2(3p_y)$ exp[e] *calc*	$2^1B_1(3p_z)$ exp[f] *calc*	1^2B_1 exp[g] *calc*
band origin		56936	52221	52648	72620
$\nu_1(a_1)$ CD stretch	2331		2237		
	2382	*2410*	*2385*	*2343*	*2335*
$\nu_2(a_1)$ NN stretch	2097		2060		
	2201	*2076*	*2221*	*2205*	*2149*
$\nu_3(a_1)$ CHD bend	1310		1305		
	1351	*1273*	*1309*	*1256*	*1297*
$\nu_4(a_1)$ CN stretch	1157		983		(960)
	1196	*751*	*1017*	*1012*	*1063*
$\nu_5(b_1)$ CNN o.p. bend	549				
	578	*565*	*448*	*455*	*434*
$\nu_6(b_1)$ CHD wag	368		(624)		
	375	*482*	*529*	*691*	*673*
$\nu_7(b_2)$ CH stretch	3133		2976		
	3262	*3307*	*3253*	*3209*	*3203*
$\nu_8(b_2)$ CHD rock					
	942	*963*	*923*	*908*	*925*
$\nu_9(b_2)$ CNN i.p. bend			326		(375)
	409	*395*	*339*	*420*	*371*

[a] All values in cm^{-1}; data from this work, unless otherwise stated. Tentatively assigned frequencies are enclosed in parentheses. [b] Data from refs 6 and 7 (frequency accuracy is ± 2 cm^{-1}). [c] Harmonic frequencies, see text. For the 1^1A_1 state, the values were calculated using B3LYP/6-311G(2df, p). For the $3^1A_1(3p_x)$ state, symmetry is lowered to C_1. [d] Uncertainty ± 15 cm^{-1}. [e] Uncertainty ± 5 cm^{-1}. [f] Fundamental frequencies from Ref 16 relative to the determined deperturbed value of the $2^1B_1(3p_z)$ band origin. The perturbed value for the band origin (52 691 cm^{-1}) was defined as the average value for the $1 \leftarrow 0$ and $0 \leftarrow 1$ transitions. [g] Frequency accuracy defined as the spacing between the rotational lines of cation is ± 50 cm^{-1}.

As far as structures are concerned, the calculated bond lengths of the neutral are within 0.002 Å of the experimental values,[28] as expected for CCSD(T)/cc-pVTZ level of theory. The B3LYP values are also very close. The maximum discrepancy between the calculated and experimental frequencies for all three isotopologes is about 5%, which is a typical value for anharmonicities. For the cation, the three lowest frequencies exhibit larger deviations, i.e., 10−12% for the CH_2 wag and CNN in-plane bend, and 37−80% for the CNN out-of-plane bend. The out-of-plane vibrations involving the carbon atom hosting the unpaired electron are similar to the out-of-plane mode in substituted methyl radicals, which has been found to be extremely anharmonic.[45] A similar trend is observed for the two Rydberg states as well—most of the calculated frequencies are within 12% from the experimental ones, except for the same out-of-plane modes, CNN out-of-plane bend and CH_2 wag.

Overall, the observed changes in structure and vibrational frequencies are consistent with removing an electron from the bonding π_{CN}-orbital, which also has an antibonding character with respect to NN. To explain the differences in structures and frequencies between the cation and the Rydberg states, we analyze the interactions of the Rydberg electron with the ion core.

For example, the $3p_y$ Rydberg orbital is localized in the plane of the molecule perpendicular to the principal rotation axis (see Figure 1 in ref 5). Its electron density is greatest on top of the hydrogen atoms and the C and middle N (directly bonded to C) atoms. The A_2 symmetry imposes a nodal plane along this axis. The $2^1A_2(3p_y)$ state differs from the cation mostly in the HCH angle (129.91° relative to 127.80° in the cation). The NBO analysis of the electron density of both states reveals that about half of the +1 charge of the nuclear core is accommodated by the hydrogens. The lobes of the $3p_y$ orbital, located directly on the hydrogen atoms in space, can interact with the positively charged hydrogen atoms. The larger HCH angle in the $2^1A_2(3p_y)$ state is thus attributed to increased electron density along the CH bonds. The $3p_y$ orbital does not affect the CN bond in a similar way due to symmetry restrictions, so the net effect is to increase repulsion between the hydrogens.

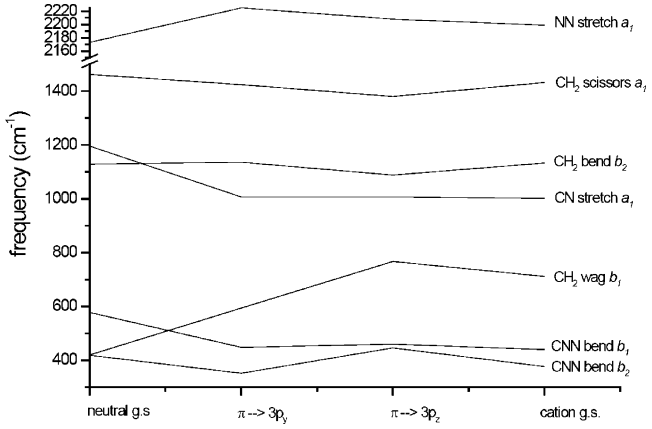

Figure 6. Harmonic frequencies of the neutral and cation ground state of CH_2N_2 compared to those of the $2^1A_2(3p_y \leftarrow \pi)$ and $2^1B_1(3p_z \leftarrow \pi)$ Rydberg excited states.

A similar argument explains the decrease in the HCH angle in the $2^1B_1(3p_z)$ state relative to the cation (124.74° compared to 127.80°). The occupied $3p_z$ orbital has electron density centered along the CNN axis, with one lobe centered directly in the space between the two hydrogens, and the other is located on the terminal nitrogen, which appropriates almost all of the remaining total nuclear positive charge. Thus, the orientation of the Rydberg orbital allows its electron density to overlap with the centers of positive charge in the nuclear core. Similar examples of Rydberg orbital orientation and the anisotropy of the cation core have been observed in a series of unsaturated hydrocarbon radicals.[46] In the $2^1B_1(3p_z)$ state of diazomethane, the HCH angle decreases to maximize this interaction. The $3p_z$ orbital, which has a node on the central nitrogen, can donate density along both the CN and NN bonds; hence the observed contraction of these bonds with respect to the cation.

The variations in the calculated vibrational frequencies for the ground-state neutral and cation, and $3p_y$ and $3p_z$ Rydberg states of CH_2N_2 are depicted in Figure 6. Only modes below 3000 cm^{-1} are shown—the frequencies of the symmetric and asymmetric CH stretches do not vary significantly with electronic excitation/ionization and are therefore omitted.

To explain the observed trends in vibrational frequencies, we divide the vibrational modes into three groups: (i) those that involve displacements mainly along the CNN framework (CN and NN stretches and CNN bends); (ii) those with displacements primarily in the CH_2 moiety (CH_2 wag, rock, and bend); and (iii) the CH stretching vibrations, which are not affected by the excitation/ionization. For the different electronic states, trends in the first group are due mostly to the effect of lower CN and NN bond orders, and those in the second are due to the interaction between the positively charged hydrogens and the Rydberg electron density, and the hybridization of the carbon. Within each group, we also observe marked differences between the in-plane and out-of-plane modes.

The four modes that comprise the first group are the CN and NN stretches (both a_1), and the b_1 and b_2 CNN bends. As shown in Figure 6, the CN stretch is strongly affected by the removal of an electron from the HOMO π orbital; whether this electron is ionized or placed in a Rydberg orbital has almost no effect on the frequency. Thus, ionization/electronic excitation results in elongation of the CN bond, and a slight contraction of the NN bond. The changes in vibrational frequencies involving CNN motions are consistent with these changes in bond order.

Referring to the out-of-plane b_1 CNN bend (ν'_5) mode, reducing the order of the π bond leads to a strong decrease in frequency in the Rydberg states as well as the cation; i.e., the in-plane Rydberg orbitals provide no additional contribution relative to the cation.

In contrast, the in-plane b_2 CNN bend (ν'_6) shows a strong frequency change between the two Rydberg states (Figure 6). The trend in this mode is complementary to that in the analogous mode in the second group—the b_2 CH_2 bend (rock). For the $3p_y$ state, the CNN bending frequency drops significantly with respect to the neutral (by 67 cm^{-1}) whereas the CH_2 bend mode increases slightly (by 7 cm^{-1}). For the $3p_z$ state, the CNN bend frequency increases relative to its value in the $2^1A_2(3p_y)$ state by 94 cm^{-1}, to above the frequency of the neutral, whereas the CH_2 bend decreases by 48 cm^{-1} to below that of the neutral. For the cation, the CNN mode drops by 69 cm^{-1} relative to the $2^1B_1(3p_z)$ state, falling again below the neutral value, and the CH_2 bend increases by 45 cm^{-1} and is, within error, the same as in the neutral. The largest difference within both modes occurs between the $2^1A_2(3p_y)$ and $2^1B_1(3p_z)$ states. For the CNN bend, the displacement moves the CNN framework off the nodal plane and into the electron density of the $3p_y$ orbital in the *yz*-plane. However, this displacement moves the atoms out of the density of the $3p_z$ orbital, which is hindered by the donation of electron density into the CN and NN bonds. Consequently, the frequency of this vibration is significantly higher in the $2^1B_1(3p_z)$ state than in the $2^1A_2(3p_y)$ state.

Finally, and quite surprisingly, the frequency of the CH_2 out-of-plane wag (ν'_6) *increases* significantly upon excitation/ionization. The reason for this is the competition between the two resonance forms in the ground-state wave function (Figure 1) and the change in hybridization of the carbon induced by ionization/electronic excitation. The NBO analysis confirms the competition between the two resonance structures in the ground-state wave function, which gives rise to sp^2 and sp^3 hybridized carbon for the left and right structures of Figure 1, respectively. Removing an electron from *either* of these structures results in sp^2 hybridized carbon and, therefore, a reduction in the sp^3 contribution, as confirmed also by NBO analysis. The increased sp^2 character leads to a stiffer out-of-plane vibration, which is exactly what is obtained in the calculations.

6. Summary

The joint experimental and theoretical investigation discusses the structure and normal-mode frequencies of the ground and excited Rydberg states of diazomethane and its isotopologs and of the corresponding cations. The experimental measurements exploit REMPI spectroscopy and velocity map imaging of photoelectrons from excited vibronic levels of the $2^1A_2(3p_y)$ state to obtain vibronic assignments in the $2^1A_2(3p_y)$ and $2^1B_1(3p_z)$ Rydberg states, and vibrational states of the cation. The accompanying high-level ab initio calculations determine structures and vibrational states in the ground states of the neutral and cations as well as the three Rydberg 3p states. The good agreement between the electronic structure results and the current experimental results on the $2^1A_2(3p_y)$ state and the cation, as well as previous studies on other states, allows a full analysis of Rydberg-ion core interactions and trends in vibrational frequencies.

Although the $2^1A_2(3p_y)$ and $2^1B_1(3p_z)$ Rydberg states have planar C_{2v} symmetry like the ion, they exhibit differences in geometry due to specific interactions of the electron in the $3p_y$ or $3p_z$ orbital with the nuclei charge distributions of the ion core. Trends in vibrational frequencies in the ground states of the neutral and ion and the $2^1A_2(3p_y)$ and $2^1B_1(3p_z)$ states are consistent with removing an electron from the bonding π_{CN}-

orbital, which nevertheless has an antibonding character with respect to NN. In explaining the observed trends, the vibrational modes are divided into two groups, which involve displacements mainly (i) along the CNN framework and (ii) in the CH_2 moiety. Trends in the first group are due mostly to effects of the lower CN and NN bond orders, whereas those in the second group are due to the interaction between the positively charged hydrogens and the Rydberg electron density, and the hybridization of the carbon. Within each group, marked differences in behavior between the in-plane and out-of-plane modes are observed. The largest changes in frequencies upon ionization are observed in the CN stretch, CH_2 wag, and the two CNN bending modes. Differences in vibrational frequencies between the $2^1A_2(3p_y)$ and $2^1B_1(3p_z)$ Rydberg states reflect state-specific interactions of the charge density of the electron in the Rydberg 3p orbital with the nuclei charge density in the ion core.

Acknowledgment. We thank Karl O. Christe and C. J. Bigler Jones for their generous help in the synthesis of the CH_2N_2 and its isotopologs. Support by the Chemical Sciences, Geosciences and Biosciences Division, Office of Basic Energy Sciences, U.S. Department of Energy (A.I.K. and H.R.) and by the Air Force Office of Scientific Research (H.R.) is gratefully acknowledged. This work was carried out in the framework of the Center for Computational Studies of Electronic Structure and Spectroscopy of Open-Shell and Electronically Excited Species (iopenshell.usc.edu) supported by the National Science Foundation through the CRIF:CRF Program.

References and Notes

(1) Kirmse, W. Ed. *Carbene Chemistry*; Academic Press: New York, 1971.

(2) Bohn, R. B.; Sandford, S. A.; Allamandola, L. J.; Cruikshank, D. P. *Icarus* **1994**, *111*, 151.

(3) Raulin, F.; Khlifi, M.; Dang-Nhu, M.; Gautier, D. *Adv. Space Res.* **1992**, *12*, 181.

(4) Moore, M. H.; Hudson, R. L. *Icarus* **2003**, *161*, 486.

(5) Fedorov, I.; Koziol, L.; Li, G. S.; Parr, J. A.; Krylov, A. I.; Reisler, H. *J. Phys. Chem. A* **2007**, *111*, 4557.

(6) Moore, C. B.; Pimentel, G. C. *J. Chem. Phys.* **1964**, *40*, 329.

(7) Moore, C. B. *J. Chem. Phys.* **1963**, *39*, 1884.

(8) Pierson, R. H.; Fletcher, A. N.; St. Clair Gantz, E. *Anal. Chem.* **1956**, *28*, 1218.

(9) Khlifi, M.; Paillous, P.; Bruston, P.; Raulin, F.; Guillemin, J. C. *Icarus* **1996**, *124*, 318.

(10) Crawford, B. L. Jr.; Fletcher Wm, H.; Ramsay, D. A. *J. Chem. Phys.* **1951**, *19*, 406.

(11) Mills, I. M.; Thompson, H. W. *Faraday Trans.* **1954**, *50*, 1270.

(12) Fletcher, Wm. H.; Garrett, Thomas, P. *J. Chem. Phys.* **1956**, *25*, 50.

(13) Vogt, J.; Winnewisser, M. *Naturforsch.* **1983**, *38a*, 1138.

(14) Vogt, J.; Winnewisser, M.; Yamada, K.; Winnewisser, G. *Chem. Phys.* **1984**, *83*, 309.

(15) Nemes, L.; Vogt, J.; Winnewisser, M. *J. Mol. Struct.* **1990**, *218*, 219.

(16) Merer, A. J. *Can. J. Phys.* **1964**, *42*, 1242.

(17) Bastide, J.; Maier, J. P. *Chem. Phys.* **1976**, *12*, 177.

(18) Sanov, A.; Droz-Georget, T.; Zyrianov, M.; Reisler, H. *J. Chem. Phys.* **1997**, *106*, 7013.

(19) Dribinski, V.; Potter, A. B.; Fedorov, I.; Reisler, H. *Chem. Phys. Lett.* **2004**, *385*, 233.

(20) Hecht, S. M.; Ozarich, J. W. *Tetrahedron Lett.* **1972**, *15*, 1501.

(21) Brinton, R. K.; Volman, D. H. *J. Chem. Phys.* **1951**, *19*, 1394.

(22) Wolf, R. J.; Hase, W. L. *J. Phys. Chem.* **1978**, *82*, 1850.

(23) Eppink, A. T. J. B.; Parker, D. H. *Rev. Sci. Instrum.* **1997**, *68*, 3477.

(24) Tanaka, Y.; Kawasaki, M.; Matsumi, Y.; Fujiwara, H.; Ishiwata, T.; Rogers, L. J.; Dixon, R. N.; Ashfold, M. N. R. *J. Chem. Phys.* **1998**, *109*, 1315.

(25) Chang, B.-Y.; Hoetzlein, R. C.; Mueller, J. A.; Geiser, J. D.; Houston, P. L. *Rev. Sci. Instrum.* **1998**, *69*, 1665.

(26) Dribinski, V.; Ossadtchi, A.; Mandelshtam, V. A.; Reisler, H. *Rev. Sci. Instrum.* **2002**, *73*, 2634.

(27) Cox, A. P; Thomas, L. F.; Sheridan, J. *Nature (London*) **1958**, *181*, 1000.

(28) Sheridan, J. *Advance in Molecular Spectroscopy*; Proceedings of the 4th International Meeting on Molecular Spectroscopy; Mangini, A. Ed.); Pergamon Press: New York 1962, Vol. I., 139.

(29) Lim, E. C. Ed. *Excited States*; Academic Press: New York 1966; Vol. III.

(30) Raghavachari, K.; Trucks, G. W.; Pople, J. A.; Head-Gordon, M. *Chem. Phys. Lett.* **1989**, *157*, 479.

(31) Watts, J. D.; Gauss, J.; Bartlett, R. J. *J. Chem. Phys.* **1993**, *98*, 8718.

(32) Dunning, T. H. *J. Chem. Phys.* **1989**, *90*, 1007.

(33) Becke, A. D. *J. Chem. Phys.* **1993**, *98*, 5648.

(34) Krishnan, R.; Binkley, J. S.; Seeger, R.; Pople, J. A. *J. Chem. Phys.* **1980**, *72*, 650.

(35) McLean, A. D.; Chandler, G. S. *J. Chem. Phys.* **1980**, *72*, 5639.

(36) Koch, H.; Jensen, H. J. Aa.; Jrgensen, P.; Helgaker, T. *J. Chem. Phys.* **1990**, *93*, 3345.

(37) Stanton, J. F.; Bartlett, R. J. *J. Chem. Phys.* **1993**, *98*, 7029.

(38) Levchenko, S. V.; Krylov, A. I. *J. Chem. Phys.* **2004**, *120*, 175.

(39) Sinha, D.; Mukhopadhyay, D.; Mukherjee, D. *Chem. Phys. Lett.* **1986**, *129*, 369.

(40) Pal, S.; Rittby, M.; Bartlett, R. J.; Sinha, D.; Mukherjee, D. *Chem. Phys. Lett.* **1987**, *137*, 273.

(41) Stanton, J. F.; Gauss, J. *J. Chem. Phys.* **1994**, *101*, 8938.

(42) Shao, Y.; Molnar, L. F.; Jung, Y.; Kussmann, J.; Ochsenfeld, C.; Brown, S.; Gilbert, A. T. B.; Slipchenko, L. V.; Levchenko, S. V.; O'Neil, D. P.; Distasio, Jr. R. A.; Lochan, R. C.; Wang, T.; Beran, G. J. O.; Besley, N. A.; Herbert, J. M.; Lin, C. Y.; Van Voorhis, T.; Chien, S. H.; Sodt, A.; Steele, R. P.; Rassolov, V. A.; Maslen, P.; Korambath, P. P.; Adamson, R. D.; Austin, B.; Baker, J.; Bird, E. F. C.; Daschel, H.; Doerksen, R. J.; Drew, A.; Dunietz, B. D.; Dutoi, A. D.; Furlani, T. R.; Gwaltney, S. R.; Heyden, A.; Hirata, S.; Hsu, C.-P.; Kedziora, G. S.; Khalliulin, R. Z.; Klunziger, P.; Lee, A. M.; Liang, W. Z.; Lotan, I.; Nair, N.; Peters, B.; Proynov, E. I.; Pieniazek, P. A.; Rhee, Y. M.; Ritchie, J.; Rosta, E.; Sherrill, C. D.; Simmonett, A. C.; Subotnik, J. E.; Woodcock, III. H. L.; Zhang, W.; Bell, A. T.; Chakraborty, A. K.; Chipman, D. M.; Keil, F. J.; Warshel, A.; Herhe, W. J.; Schaefer, H. F., III; Kong, J.; Krylov, A. I.; Gill, P. M. W.; Head-Gordon, M. *Phys. Chem. Chem. Phys.* **2000**, *8*, 3172.

(43) Stanton, J. F.; Gauss, J.; Watts, J. D.; Lauderdale, W. J.; Bartlett, R. J. *ACES II*, 1993. The package also contains modified versions of the MOLECULE Gaussian integral program of J. Almlöf and P. R. Taylor, the ABACUS integral derivative program written by T. U. Helgaker, H. J. Aa. Jensen, P. Jørgensen, and T. P. Taylor, and the PROPS property evaluation integral code of P. R. Taylor.

(44) Glendening, E. D.; Badenhoop, J. K.; Reed, A. E.; Carpenter, J. E.; Bohmann, J. A.; Morales, C. M.; Weinhold, F. *NBO 5.0*; Theoretical Chemistry Institute, University of Wisconsin: Madison, WI, 2001.

(45) Levchenko, S. V.; Demyanenko, A. V.; Dribinski, V. L.; Potter, A. B.; Reisler, H.; Krylov, A. I. *J. Chem. Phys.* **2003**, *118*, 9233.

(46) Koziol, L.; Levchenko, S.; Krylov, A. I. *J. Phys. Chem. A* **2006**, *110*, 2746.